Eddy-current probe impedance due to a volumetric flaw

J. R. Bowler and S. A. Jenkins
University of Surrey, Guildford, Surrey GU2 5XH, United Kingdom

L. D. Sabbagh and H. A. Sabbagh
Sabbagh Associates, Inc., 4639 Morningside Drive, Bloomington, Indiana 47401

(Received 11 December 1990; accepted for publication 25 January 1991)

Eddy current induced in a metal by a coil carrying an alternating current may be perturbed by the presence of any macroscopic defects in the material, such as cracks, surface indentations, or inclusions. In eddy-current nondestructive evaluation, defects are commonly sensed by a change of the coil impedance resulting from perturbations in the electromagnetic field. This paper describes theoretical predictions of eddy-current probe responses for surface cracks with finite opening. The theory expresses the electromagnetic field scattered by a three-dimensional flaw as a volume integral with a dyadic kernel. Probe signals are found by first solving an integral equation for the field at the flaw. The field equation is approximated by a discrete form using the moment method and a numerical solution found using conjugate gradients. The change in probe impedance due to a flaw is calculated from the flaw field. Predictions of the theory are compared with experimental impedances due to eddy-current interaction with a rectangular surface breaking slot. Good agreement is found between predictions and the measurements.

I. FLAW EXCITATION

In a well-known early study of eddy-current nondestructive evaluation (NDE),[1] Burrows pointed out that the perturbed field due to a small flaw, such as a spheroidal cavity in a conductor-carrying eddy current, is the same as the field of an embedded current dipole. The idea of representing the effect of a small flaw by a point source has parallels in other branches of applied physics. For example far-field scattering of an electromagnetic wave is frequently represented as a multipole expansion; the dipole term being the one that decays most slowly with distance from the scatterer. In eddy-current NDE however, far-field behavior is of limited practical interest since the probe and the flaw must be close together to guarantee reliable detection. Fortunately it is possible to treat near-field effects of a finite flaw in terms of a distributed source. If the flaw is a thin crack modeled as a surface barrier to eddy current, then the crack behaves as a surface layer of current dipoles.[2] Here three-dimensional flaws in nonferromagnetic materials are considered, their equivalent source being volume current dipole distributions.

The induced dipole moment at the flaw depends on the incident electromagnetic field, the flaw parameters, and the presence of an interface between the conductor and the surrounding air. Any calculation of the dipole density must take account of the mutual interaction between dipoles. In our integral equation formulation, a dyadic integral kernel represents the interaction between different parts of the source. The mutual interaction between dipoles takes place both directly and via reflections from the surface of the conductor. Therefore, the dyadic Green's kernel contains both direct and reflection terms. It ensures that whatever flaw is considered, the perturbed field satisfies the correct continuity conditions at the conductor/air interface and vanishes as the radial field coordinate goes to infinity. Because these conditions are automatically satisfied, one is free to concentrate on evaluating the field at the flaw. This has computational advantages since only the flaw region needs to be made discrete, thus limiting the required number of unknowns. One possible alternative would be to use a free-space or unbounded domain Green's function. An application of Green's second theorem would yield surface integrals at the interface and these would have to be included in any numerical scheme, possibly using boundary elements. Consequently the number of unknowns would have to increase. Choosing a dyad that embodies the conductor/air interface conditions removes the need for a surface term but places a restriction on the conductor geometry we can study since the required Green's functions are only available in explicit form for simple structures such as a layered half-space, an infinite cylinder, or a sphere.[3] In the present analysis an isotropic homogeneous half-space conductor is considered.

The method of moments is used here to approximate the integral equation for the dipole distribution by a discrete equation.[4] A similar approach has been used by McKirdy[5] to determine the electric field at a slot in a conductor. The discrete equation is then solved to get a piecewise constant approximation of the dipole density at the flaw. With the flaw region divided into say N volumetric cells and three dipole components for each cell, it is necessary to solve a linear system with $3N$ unknowns. Although the number of unknowns needed in a typical eddy-current NDE problem may not be large, possibly a few hundred, a numerical algorithm has been designed with a view to treating very large systems of equations and adapting it for other applications such as microwave scattering at penetrable bodies. Based on this strategy the linear system is solved iteratively using a conjugate-gradient algorithm. The matrix-vector products that consume most of the computational effort in the conjugate-gradient scheme

 0021-8979/91/031107-08$03.00 © 1991 American Institute of Physics

Downloaded 10 May 2004 to 129.186.200.45. Redistribution subject to AIP license or copyright, see http://jap.aip.org/jap/copyright.jsp

are computed using fast Fourier transforms.[6]

Once the effective source strength of the flaw is known, it is easy to calculate the change of probe impedance due to the scattered field. One possible method for finding the probe response is to determine first the scattered electric field at the probe coil and then integrate over the coil region to give the impedance contribution from the scattered field alone. However, by using a reciprocity theorem,[7] it is possible to show that the same result may be found from an integral over the flaw. This second integral is much more convenient to use since the integrand is the dot product of the incident electric field and the induced source distribution, making it unnecessary to perform the intermediate step of computing the scattered field at the excitation coil. In the discrete problem, where there are $3N$ unknowns, the impedance integral is approximated very simply by a $3N$-dimensional scalar product and is computed very rapidly.

II. INTEGRAL FORMULATION

In a previous study, a volume integral formulation was used to calculate the induced magnetization of ferrite eddy current probe cores.[8] Viewed as a scattering problem, the coil current produces an incident magnetic field and the core acts as the scatterer. The induced magnetic dipole moment of the ferrite core is then regarded as the source of the scattered field. A Fredholm integral equation of the second kind expresses the total magnetic field as the sum of the incident field due to the coil and the scattered field due to the core. Assuming the core has linear material properties leads to an equation for the core magnetization. This equation is then approximated by a discrete form by subdividing the core into volume elements and a numerical solution computed giving the core magnetization of each element. Although the flaw problem is physically different, the same basic formulation may be adopted to determine the induced source strength at an inhomogeneity in a conductor-carrying eddy current. Assuming the conductor is nonferromagnetic, the induced source at the defect is an electric current dipole moment. We shall develop an integral equation for the current dipole density beginning with the fundamental equations of linear electromagnetic theory.

Assuming an excitation varying in time as the real part of $\exp(-i\omega t)$, Maxwell's equations for an isotropic conductor containing a local conductivity variation may be written as

$$\begin{aligned}\nabla\times\mathbf{E}(\mathbf{r})&=i\omega\mu_0\mathbf{H}(\mathbf{r}),\\ \nabla\times\mathbf{H}(\mathbf{r})&=\sigma(\mathbf{r})\mathbf{E}(\mathbf{r}),\\ &=\sigma_0\mathbf{E}(\mathbf{r})+\mathbf{P}(\mathbf{r}),\end{aligned}\tag{1}$$

where diplacement current is neglected. $\mathbf{P}(\mathbf{r})L=[\sigma(\mathbf{r})-\sigma_0]\mathbf{E}(\mathbf{r})$ is the induced current dipole density at the flaw due to departures from an otherwise constant conductivity σ_0. The flaw calculation is developed from a solution of Maxwell's equations expressed using the electric-electric dyadic Green's function $\mathbf{G}(\mathbf{r}|\mathbf{r}')$ as[3]

$$\mathbf{E}(\mathbf{r})=\mathbf{E}^{(i)}(\mathbf{r})+i\omega\mu_0\int_{\text{flaw}}\mathbf{G}(\mathbf{r}|\mathbf{r}')\cdot\mathbf{P}(\mathbf{r}')d\mathbf{r}',\tag{2}$$

where $\mathbf{E}^{(i)}(\mathbf{r})$ is the incident or unperturbed field and the integral represents the electric field scattered by the flaw. $\mathbf{G}(\mathbf{r}|\mathbf{r}')$ transforms an electric source into an electric field hence its designation as an electric-electric Green's function. It is a solution of

$$\nabla\times\nabla\times\mathbf{G}(\mathbf{r}|\mathbf{r}')-k^2\mathbf{G}(\mathbf{r}|\mathbf{r}')=\delta(\mathbf{r}-\mathbf{r}')\mathbf{I},\tag{3}$$

satisfying the same boundary and interface conditions as the electric field. $\mathbf{I}=\hat{x}\hat{x}+\hat{y}\hat{y}+\hat{z}\hat{z}$ is the unit tensor here expressed in terms of unit vectors, $\mathbf{r}'$ is the coordinate of a source point in a half-space conductor ($z'<0$) and $L\ k^2=i\omega\mu_0\sigma_0$. The half-space solution of Eq. (3) can be derived by a scalar decomposition of the field and Fourier transformation of the field equations, an approach previously used for the analysis of external sources.[9] This approach leads to a result equivalent to that derived by Riache and Coggon.[10] Assuming that the Green's functions vanish as $|\mathbf{r}|\to\infty$, scalar decomposition gives the form

$$\begin{aligned}\mathbf{G}(\mathbf{r}|\mathbf{r}')&=\mathbf{G}_0(\mathbf{r}|\mathbf{r}')+\mathbf{G}_i(\mathbf{r}|\mathbf{r}')\\ &\quad+(1/k^2)\nabla\times\hat{z}\nabla'\times\hat{z}\mathbf{V}(\mathbf{r}|\mathbf{r}'),\end{aligned}\tag{4}$$

where $\mathbf{G}_0(\mathbf{r}|\mathbf{r})$ is the dyadic Green's function for an unbounded conductor given by

$$\mathbf{G}_0(\mathbf{r}|\mathbf{r}')=[\mathbf{I}+(1/k^2)\nabla\nabla]\phi(\mathbf{r}|\mathbf{r}'),\tag{5}$$

with

$$\phi(\mathbf{r}|\mathbf{r}')=\frac{e^{ik|\mathbf{r}-\mathbf{r}'|}}{4\pi|\mathbf{r}-\mathbf{r}'|},\tag{6}$$

and the two remaining terms in Eq. (4) are due to reflection at the surface of the material. The first of these is the image term,

$$\mathbf{G}_i(\mathbf{r}|\mathbf{r}')=[\mathbf{I}'-(1/k^2)\nabla\nabla']\phi(\mathbf{r}|\mathbf{r}''),\tag{7}$$

where $\mathbf{r}''=\mathbf{r}'-2\hat{z}z'$ is the image point and $\mathbf{I}'=\hat{x}\hat{x}+\hat{y}\hat{y}-\hat{z}\hat{z}$. The second contains a function $V(\mathbf{r}|\mathbf{r}')$ given by the Fourier integral

$$V(\mathbf{r}|\mathbf{r}')=-\frac{k^2}{(2\pi)^2}\int_{-\infty}^{\infty}\int_{-\infty}^{\infty}\frac{1}{\kappa\gamma(\kappa+\gamma)}\times e^{-\gamma|z+z'|+iu(x-x')+iv(y-y')}\,du\,dv.\tag{8}$$

Here u and v are Fourier space coordinates, $L\ \kappa=(u^2+v^2)^{1/2}$, and $\gamma=(u^2+v^2-k^2)^{1/2}$, where the L roots with positive real parts are taken.

Alternative representations of $V(\mathbf{r}|\mathbf{r}')$ may be found by writing its Fourier transform with respect to x and y in two parts as

$$1/\kappa\exp(-\gamma|z+z'|)-1/\gamma\exp(-\gamma|z+z'|),$$

and defining a function $L(k,\rho,\zeta)$ given by

$$L(k,\rho,\zeta)=\frac{1}{2\pi}\int_{-\infty}^{\infty}\int_{-\infty}^{\infty}\frac{1}{\kappa\gamma}\times e^{-\gamma\zeta+iu(x-x')+iv(y-y')}\,du\,dv,\tag{9}$$

Downloaded 10 May 2004 to 129.186.200.45. Redistribution subject to AIP license or copyright, see http://jap.aip.org/jap/copyright.jsp

where $\rho^2=(x-x')^2+(y-y')^2$ and $\zeta=|z+z'|$. Then

$$V(\mathbf{r}|\mathbf{r}')=\pm\frac{1}{2\pi}\frac{\partial}{\partial z}L(k,\rho,|z+z'|)-2\phi(\mathbf{r}|\mathbf{r}''), \tag{10}$$

where the $+$ sign holds if $z+z'<0$ and the $-$ sign if $z+z'>0$. In writing Eq. (10) the Fourier representation

$$\phi(\mathbf{r}|\mathbf{r}')=\frac{1}{(2\pi)^2}\int_{-\infty}^{\infty}\int_{-\infty}^{\infty}\frac{1}{2\gamma}\times e^{-\gamma|z-z'|+iu(x-x')+iv(y-y')}\,du\,dv, \tag{11}$$

for the scalar Green's function has been adapted for a singular source at the image point. Note also that Eq. (9), referred to by Banos as the Foster–Lien integral,[11] may be written in terms of modified Bessel functions as[12]

$$L(k,\rho,\zeta)=\int_0^{\infty}\frac{1}{\gamma}e^{-\gamma\zeta}J_0(\rho s)ds=I_0[-ik(S-\zeta)/2]K_0[-ik(S+\zeta)/2], \tag{12}$$

where $S^2=\rho^2+\zeta^2$. Here we have taken $L(-k^2)^{-1/2}=-ik$ since the arguments of the modified Bessel functions must have a positive real part. Because the arguments have real and imaginary parts of equal magnitude, the modified Bessel functions can be written in terms of Kelvin functions. To evaluate the last term in Eq. (4), $V(\mathbf{r}|\mathbf{r}')$ is differentiated and the result expressed in terms of Kelvin functions. For numerical coding the Kelvin functions are approximated using polynonials.[13]

Suppose we define the flaw function $v(\mathbf{r})$ as $L\,v(\mathbf{r})=[\sigma(\mathbf{r})-\sigma_0]/\sigma_0$, then multiplying Eq. (2) by $L\,\sigma_0 v(\mathbf{r})$ gives

$$\mathbf{P}(\mathbf{r})=\mathbf{P}^{(i)}(\mathbf{r})+v(\mathbf{r})k^2\int_{\text{flaw}}\mathbf{G}(\mathbf{r}|\mathbf{r}')\cdot\mathbf{P}(\mathbf{r}')d\mathbf{r}'. \tag{13}$$

$\mathbf{P}^{(i)}(\mathbf{r})=\sigma_0 v(\mathbf{r})\mathbf{E}^i(\mathbf{r})$ and therefore vanishes at points not on the flaw. By solving Eq. (13) we obtain the effective source distribution of the flaw for a given excitation $\mathbf{P}^{(i)}\mathbf{P}^{(i)}(\mathbf{r})$. Then the probe impedance or the scattered field are easily found from the induced source strength at the scatterer. Because we are interested in finding approximate numerical solutions that will give good results for an arbitrary flaw geometry, we have chosen to use the moment method to determine $\mathbf{P}(\mathbf{r})$, approximating Eq. (13) by a matrix equation.

III. DISCRETIZATION OF THE INTEGRAL EQUATION

A discrete approximation of the integral equation (13) is found by subdividing the region of space occupied by the flaw into a regular lattice of $N_x\times N_y\times N_z$ cells, each cell being a rectangular parallelepiped of equal size $\delta_x\times\delta_y\times\delta_z$. The induced current dipole density and the flaw function are then expanded as pulse functions defined over the grid. Thus

$$\mathbf{P}(\mathbf{r})=\sum_{l=0}^{N_x-1}\sum_{m=0}^{N_y-1}\sum_{j=0}^{N_z-1}\mathbf{P}_{lmj}P_l\left(\frac{x-x_0}{\delta_x}\right)\times P_m\left(\frac{y-y_0}{\delta_y}\right)P_j\left(\frac{z-z_0}{\delta_z}\right), \tag{14}$$

and

$$v(\mathbf{r})=\sum_{l=0}^{N_x-1}\sum_{m=0}^{N_y-1}\sum_{j=0}^{N_z-1}v_{lmj}P_l\left(\frac{x-x_0}{\delta_x}\right)\times P_m\left(\frac{y-y_0}{\delta_y}\right)P_j\left(\frac{z-z_0}{\delta_z}\right), \tag{15}$$

x_0, y_0, and z_0 being reference coordinates for the source grid. The pulse function $P_j(s)$, is defined by

$$P_j(s)=\begin{cases}1, & \text{if } j-\frac{1}{2}\leqslant s<j+\frac{1}{2}\\ 0, & \text{otherwise.}\end{cases} \tag{16}$$

Thus an arbitrary defect is modeled by assigning suitable values of v_{lmk} on a regular rectangular lattice and postulating that the dipole source density is constant within each individual cell. For a crack or cavity of zero conductivity it follows from the definition that values of v_{lmj} will be -1.0 for cells totally within the flaw. Where a cell is external to the flaw the discrete flaw function is zero and for cells on the boundary, some appropriate intermediate value is assigned. Discretization error will be reduced by defining the flaw with a smaller cell size and a larger number of cells but this must be offset against a higher computational cost.

To complete the discretization, the same three-dimensional pulse functions adopted for expanding the unknown are used for testing. Testing is carried out by multiplying the integral equation by the testing functions and integrating over the field coordinates. That is, we take moments of the field by multiplying Eq. (13) by

$$P_l\left(\frac{x-x_0}{\delta_x}\right)P_m\left(\frac{y-y_0}{\delta_y}\right)P_j\left(\frac{z-z_0}{\delta_z}\right)/\delta_x\delta_y\delta_z,$$

and then integrating with respect to x, y, and z. This procedure yields a linear system for the solution vector $\mathbf{P}_{lmj}$ given by

$$\mathbf{P}^{(i)}_{lmj}=\mathbf{P}_{lmj}-v_{lmj}\sum_{L=0}^{N_x-1}\sum_{M=0}^{N_y-1}\sum_{J=0}^{N_z-1}\mathbf{G}_{jkl,\,JKL}\cdot\mathbf{P}_{LMJ}, \tag{17}$$

where $\mathbf{P}^{(i)}_{klm}$ is given in terms of the unperturbed electric field in the flaw region due to the probe as

$$\mathbf{P}^{(i)}_{klm}=\frac{\sigma_0 v_{klm}}{\delta_x\delta_y\delta_z}\int_{x_k}^{x_{k+1}}\int_{x_l}^{x_{l+1}}\int_{z_m}^{z_{m+1}}\mathbf{E}^{(i)}(\mathbf{r})dx\,dy\,dz. \tag{18}$$

Downloaded 10 May 2004 to 129.186.200.45. Redistribution subject to AIP license or copyright, see http://jap.aip.org/jap/copyright.jsp

Here $x_k=k\delta_x+x_0$, $y_l=l\delta_y+y_0$, and $z_m=m\delta_z+z_0$, etc. $(k,l,m=0,1,2,3...)$. The dimensionless matrix in Eq. (17) is given by

$$\mathbf{G}_{klm,KLM}=k^2\int_{x_{k-1}}^{x_{k+1}}\int_{y_{l-1}}^{y_{l+1}}\int_{z_{m-1}}^{z_{m+1}}\mathbf{G}(x_k,y_l,z_m|x',y',z')\times\beta_K\left(\frac{x'-x_0}{\delta_x}\right)\times\beta_L\left(\frac{y'-y_0}{\delta_y}\right)\beta_M\left(\frac{z'-z_0}{\delta_z}\right)dx'\,dy'\,dz', \quad (19)$$

where $\beta_j(u)$, $(j=0,1,2,3...)$ is a convolution of pulse functions given by

$$\beta_j(s)=\begin{cases}-|j-s|+1, & \text{if } j-1\leqslant s<j+1,\\ 0, & \text{otherwise.}\end{cases} \quad (20)$$

The matrix elements have been computed from Eq. (19) using a numerical quadrature scheme for three-dimensional integration.[14] Singular matrix elements are calculated by enclosing the singularity in a finite exclusion volume chosen to be a cube whose sides are of length $2a$. Integration over the exclusion volume is based on a regularization scheme suggested by Lee, *et al.*[15] for dealing with the strong singularity in the dyadic Green's function. By approximating the exponential term in the free-space Green's function by a Taylor's series expansion and integrating term by term, the exclusion volume integral is expressed in the form of a power-series expansion in ak. Because the size of the exclusion volume is chosen to be much less than the skin depth, the product ak is small and only a few terms in the polynomial are required to get reasonable accuracy, typically 3–5. The singular matrix element is found by adding the exclusion volume integral to the result of integrating over the remainder of the singular cell using a numerical quadrature scheme. The sum of the two contributions should be independent of the exclusion volume size allowing a useful check on the result. Details of this calculation are described in a separate article.[16]

IV. UNPERTURBED FIELD

The excitation vector $\mathbf{P}_{klm}^{(i)}$ is given in terms of the unperturbed electric field at the flaw by Eq. (18). In general the incident electric field in the conductor due to an arbitrary external current source $\mathbf{J}(\mathbf{r})$ is given by an equation of the form

$$\mathbf{E}^{(i)}(\mathbf{r})=\frac{i\omega\mu_0}{4\pi^2}\int_{\text{coil}}dz'\int\int_{-\infty}^{\infty}\tilde{\mathbf{G}}_T(z|z')\cdot\tilde{\mathbf{J}}(z')\times e^{i(ux+vy)}\,du\,dv, \quad (21)$$

where $\tilde{\mathbf{G}}_T$ transforms an external electric current source into the electric field in the conductor. The transmission dyadic function transforms the external current source into a transverse electric field and may be written as[9]

$$\mathbf{G}_T(\mathbf{r}|\mathbf{r}')=\nabla\times\hat{\mathbf{z}}\nabla\times'\hat{z}U(\mathbf{r}|\mathbf{r}'), \quad (22)$$

where $U(\mathbf{r}|\mathbf{r}')$ is a transverse electric potential given by

$$\nabla_t U(\mathbf{r}|\mathbf{r}')=\frac{1}{(2\pi)^2}\int_{-\infty}^{\infty}\int_{-\infty}^{\infty}\frac{i(u\hat{x}+v\hat{y})}{\kappa^2(\kappa+\gamma)}\times e^{\gamma z-\kappa z'+iu(x-x')+iv(y-y')}\,du\,dv, \quad (23)$$

where $\nabla_t=\nabla-\hat{z}\partial/\partial z$. Hence the Fourier transform of the transmission Green's function is

$$\tilde{\mathbf{G}}_T(z|z')=\begin{bmatrix}v^2 & -uv & 0\\ -uv & u^2 & 0\\ 0 & 0 & 0\end{bmatrix}\frac{1}{\kappa^2(\kappa+\gamma)}e^{\gamma z-\kappa z'}. \quad (24)$$

For a normal cylindrical coil with a relatively large uniform turns density n, the coil current density may be approximated as uniform and azimuthal over a finite region. Using cylindrical polar coordinates to define the coil current density $\mathbf{J}$, with $\mathbf{a}_\phi$ as a unit azimuthal vector and I as the current per turn, we have

$$\mathbf{J}(\rho,z,\phi)=\begin{cases}a_\phi nI, & z_a\leqslant z\leqslant z_b \text{ and } \rho_1\leqslant\rho\leqslant\rho_2,\\ 0, & \text{otherwise,}\end{cases} \quad (25)$$

where ρ_1 is the inner radius and ρ_2 the outer radius of the coil. z_a and z_b are its lower and upper limits. The induced field $\mathbf{E}^{(i)}(\mathbf{r})$ is evaluated through the two-dimensional Fourier transform of the current density. Assuming that the coil axis is located at (x_c,y_c), the required transform of Eq. (25) is

$$\tilde{\mathbf{J}}(z)=\begin{cases}i2\pi nI\left(\hat{x}\frac{v}{\kappa}-\hat{y}\frac{u}{\kappa}\right)[\rho_2^2\mathscr{T}(\kappa\rho_2)-\rho_1^2\mathscr{T}(\kappa\rho_1)]\\ \times e^{-i(ux_c+vy_c)} \quad z_a\leqslant z\leqslant z_b\\ 0 \quad \text{otherwise.}\end{cases} \quad (26)$$

The function $\mathscr{T}(s)$, which arises in taking the Bessel transform of Eq. (25), is defined by[17]

$$\mathscr{T}(s)=\int_0^1\rho J_1(\rho s)\,d\rho=\frac{\pi}{2s}[J_1(s)\mathbf{H}_0(s)-J_0(s)\mathbf{H}_1(s)], \quad (27)$$

where J_0 and J_1 are Bessel functions of the first kind. $\mathbf{H}_0$ and $\mathbf{H}_1$ are Struve functions.

To determine the excitation vector $\mathbf{P}_{lmk}^{(i)}$ explicitly for a normal cylindical coil, Eqs. (21), (24), and (26) are combined with with Eq. (18) to give

Downloaded 10 May 2004 to 129.186.200.45. Redistribution subject to AIP license or copyright, see http://jap.aip.org/jap/copyright.jsp

$$\mathbf{P}^{(i)}_{lmk}=\frac{-inIk^2v_{lmk}}{2\pi\delta_z}\int_{-\infty}^{\infty}\int_{-\infty}^{\infty}\frac{\rho_2^2\mathscr{T}(\kappa\rho_2)-\rho_1^2\mathscr{T}(\kappa\rho_1)}{\kappa^2\gamma(\kappa+\gamma)}$$
$$\cdot\begin{bmatrix}v\\-u\\0\end{bmatrix}\cdot(e^{-\kappa z_b}-e^{-\kappa z_a})$$
$$\times(e^{\gamma z_{k+1}}-e^{\gamma z_k})\cdot\frac{\sin(u\delta_x/2)}{u\delta_x/2}$$
$$\times\frac{\sin(v\delta_y/2)}{v\delta_y/2}e^{i[u(\delta_x l-x_0-x_c)+v(\delta_y m-y_0-y_c)]}\,du\,dv. \tag{28}$$

For computational efficiency, the double integral is evaluated using a two-dimensional Fast Fourier transform (FFT).

V. FLAW IMPEDANCE

Adopting the probe current as the phase reference, the probe impedance ΔZ due to the flaw, expressed in terms of the electric field $\mathbf{E}^{(s)}(\mathbf{r})$ scattered by the flaw, is given by

$$I^2\Delta Z=-\int_{\text{coil}}\mathbf{E}^{(s)}(\mathbf{r})\cdot\mathbf{J}(\mathbf{r})d\mathbf{r}. \tag{29}$$

One might use Eq. (29) directly to compute the probe response but this would entail the intermediate step of calculating the scattered field at the coil before integrating over the coil region to get the impedance. Instead we apply a reciprocity theorem relating the scattered field at the primary source (the eddy-current probe) to the incident field at the secondary source (the induced current dipole density at the flaw). A similar form of the reciprocity principle is used to determine antennae impedances.[7] Thus,

$$I^2\Delta Z=-\int_{\text{flaw}}\mathbf{E}^{(i)}(\mathbf{r})\cdot\mathbf{P}(\mathbf{r})d\mathbf{r}. \tag{30}$$

Transforming to a discrete form, $\mathbf{P}(\mathbf{r})$ is again approximated by a pulse function sum as in Eq. (14) and the flaw integration carried out over each volume element to give

$$I^2\Delta Z=-\delta_x\delta_y\delta_z\sum_{k=0}^{N_x-1}\sum_{l=0}^{N_y-1}\sum_{m=0}^{N_z-1}\times\mathbf{P}^{(i)}_{klm}\cdot\mathbf{P}_{klm}/(\sigma_0 v_{klm}). \tag{31}$$

Equation (31) allows us to compute the change in probe impedance due to the flaw from the solution vector as a simple multidimensional scalar product.

VI. NUMERICAL ALGORITHM

Approximate solutions of the discrete problem, Eq. (17), have been calculated using a conjugate-gradient algorithm.[17,18] In this and similar algorithms, the greatest computational expense is incurred in the calculation of matrix vector products; therefore, it is important that these L products are evaluated efficiently. The demand for computational efficiency is particularly acute where there is a need to obtain accurate numerical results because the discrete problem must have a fine resolution to make discretization errors small. In a three-dimensional vector calculation such as this, the required number of unknowns may have to be very large to keep discretization errors within tolerable limits. Using a large number of elements could mean that the memory and processing requirements of the computation are prohibitive. Fortunately the Green's function has a convolutional-correlational structure that is preserved in a discrete form by choosing a regular array of similar volume elements. Not only is the integral in Eq. (13) a convolution in x and y, it may also be written as the sum of a convolution in z and a correlation in z, corresponding to the free-space and reflection parts of the Green's function, respectively. The correlation in z is recognizable from the $z+z'$ dependence of $\mathbf{G}_i(\mathbf{r}|\mathbf{r}')$, Eq. (7), and $V(\mathbf{r}|\mathbf{r}')$, Eq. (8). As a consequence, there is first a redundancy in the matrix (19) allowing a reduction in storage requirements and second a Toeplitz–Hankel structure that allows matrix-vector products to be calculated using FFTs.

In order to apply conjugate gradients in calculating the current dipole density at the flaw, Eq. (17) is interpreted as a matrix equation whose matrix elements are Cartesian tensors. In this scheme the elements of $\mathbf{P}_{lmj}$ have three components and the v_{lmj} are scalar row multipliers. In operator form we have

$$Y=\mathscr{A}X, \tag{32}$$

where

$$Y\equiv\mathbf{P}^{(i)}_{lmj},\quad X\equiv\mathbf{P}_{lmj}, \tag{33}$$

and

$$\mathscr{A}X=\mathbf{P}_{lmj}-v_{lmj}\sum_{J=0}^{N_x-1}\sum_{L=0}^{N_x-1}\sum_{M=0}^{N_y-1}\mathbf{G}_{lmj,LMJ}\mathbf{P}_{LMJ}. \tag{34}$$

Also needed is the adjoint operator, $\mathscr{A}^\dagger$,[18,19] given by

$$\mathscr{A}^\dagger X=\mathbf{P}_{lmj}-\sum_{J=0}^{N_z-1}\sum_{L=0}^{N_x-1}\sum_{M=0}^{N_y-1}\mathbf{G}^T_{lmj,LMJ}v_{LMJ}\mathbf{P}_{LMJ}. \tag{35}$$

The superscript T here denotes the conjugate transpose of a dyad. Note that v_{lmj} are real numbers, therefore conjugation leaves these unchanged.

The conjugate-gradient algorithm begins with an initial guess or estimate X_0 from which we compute L $R_0=Y-\mathscr{A}X_0$, and $P_1=Q_0=\mathscr{A}^\dagger R_0$. A convergence parameter ϵ determines the point at which the desired accuracy has been achieved. If k is the iteration number, then the algorithm proceeds as follows; for $k=1,2,\ldots$, if L Test $=\|R_k\|/\|Y\|<\epsilon$, stop. X_k is then the optimal solution of Eq. (32). Otherwise, update X_k by the following steps:

$$\begin{aligned}&S_k=\mathscr{A}P_k,\\&a_k=\|Q_{k-1}\|^2/\|S_k\|^2,\\&X_k=X_{k-1}+a_kP_k,\\&R_k=R_{k-1}-a_kS_k,\\&Q_k=\mathscr{A}^\dagger R_k,\end{aligned} \tag{36}$$

Downloaded 10 May 2004 to 129.186.200.45. Redistribution subject to AIP license or copyright, see http://jap.aip.org/jap/copyright.jsp

TABLE I. Experimental probe-flaw interaction parameters.

Coil parameters	
Inner radius (ρ_1)	6.15 ± 0.05 mm
Outer radius (ρ_2)	12.4 ± 0.05 mm
Length ($z_b - z_a$)	6.15 ± 0.1 mm
Number of turns	3790
Liftoff (z_a)	0.88 mm
Frequency	900 Hz
Specimen parameters	
Conductivity (σ)	$3.06 \pm 0.02 \times 10^7$ s/m
Thickness	12.22 ± 0.02 mm
Flaw parameters	
Length (2 c)	12.60 ± 0.02 mm
Depth (h)	5.00 ± 0.05 mm
Width (w)	0.28 ± 0.01 mm

$$b_k = \|Q_k\|^2 / \|Q_{k-1}\|^2,$$

$$P_{k+1} = b_k P_k + Q_k.$$

The numerical convolution and correlations implied by the operation $\mathscr{A} P_k$ and $\mathscr{A}^\dagger R_k$ are performed efficiently by using the FFT. This, together with the fact that the storage requirements are reasonably modest, are the reasons why the conjugate-gradient algorithm is attractive for large systems of equations with Toeplitz and/or Hankel forms.

VII. PREDICTIONS AND COMPARISON WITH EXPERIMENT

We have calculated the impedance change of a cylindrical coil due to a rectangular surface slot in a conductor and compared these predictions of the model with the benchmark experimental measurements made by Burke.[20] The coil, specimen, and flaw parameters for the benchmark experiment are given in Table I. Although the measurements were made on a finite slab of aluminium alloy, the calculations assume a half-space conductor. However, because the skin depth in these experiments (3.04 mm) is only 25% of the plate thickness at the test frequency (900 Hz), this assumption should not produce significant errors in the predictions. The lift-off parameter z_a, the distance from the base of the coil to the surface of the workpiece, is held constant at 0.88 mm.

Figure 1 shows the excitation coil in relation to the slot and the coordinate system used to define the probe position. Impedance measurements made with the coil position varied in the plane of the slot are compared with theoretical results in Figs. 2 and 3. Figure 2 shows the variation in the absolute value of the coil impedance change and Fig. 3 shows the phase variation. At $x=0$ the coil axis passes through the center of the slot and, because the mean diameter of the coil is greater than the slot length, the eddy current circulates around the defect without interacting strongly. The greatest interaction is observed when the coil

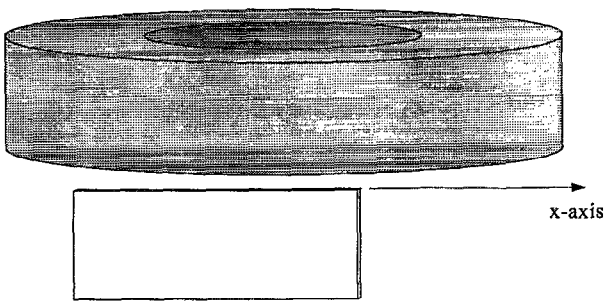

FIG. 1. Eddy-current coil over a rectangular surface slot in a conducting half-space.

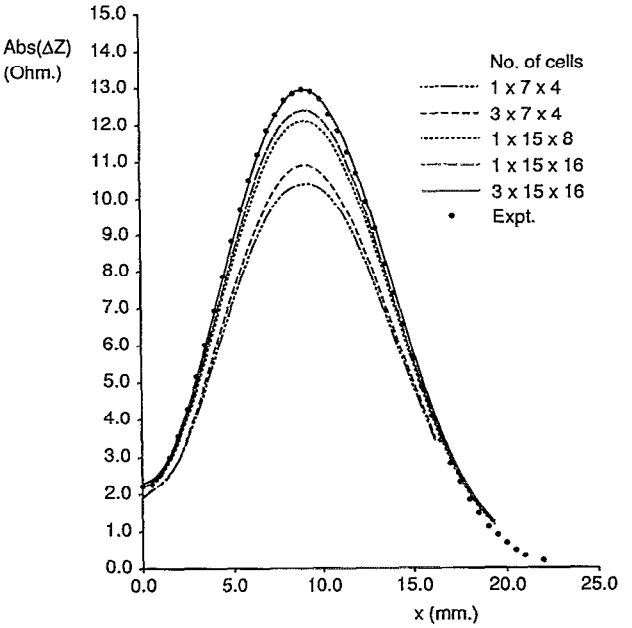

FIG. 2. Comparison of predicted absolute impedance with experiment. Variation of $|\Delta Z|$ with distance measured along the slot from its center.

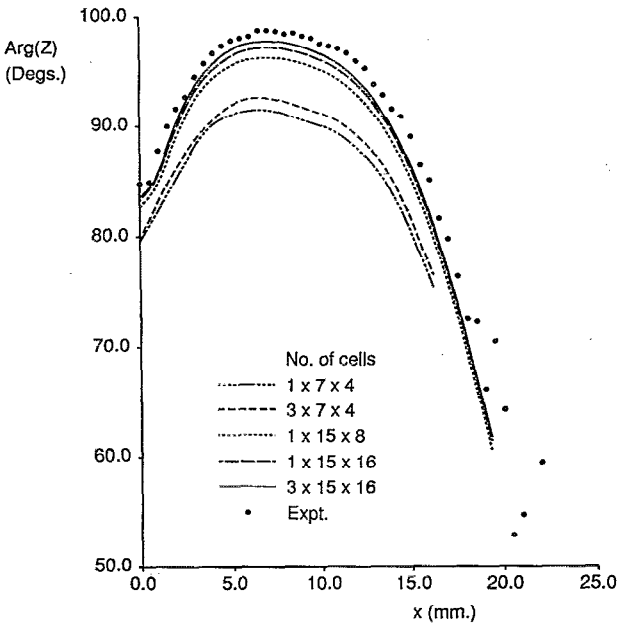

FIG. 3. Comparison of phase with experiment. Variation of arg(ΔZ) with distance measured along the slot from its center.

Downloaded 10 May 2004 to 129.186.200.45. Redistribution subject to AIP license or copyright, see http://jap.aip.org/jap/copyright.jsp

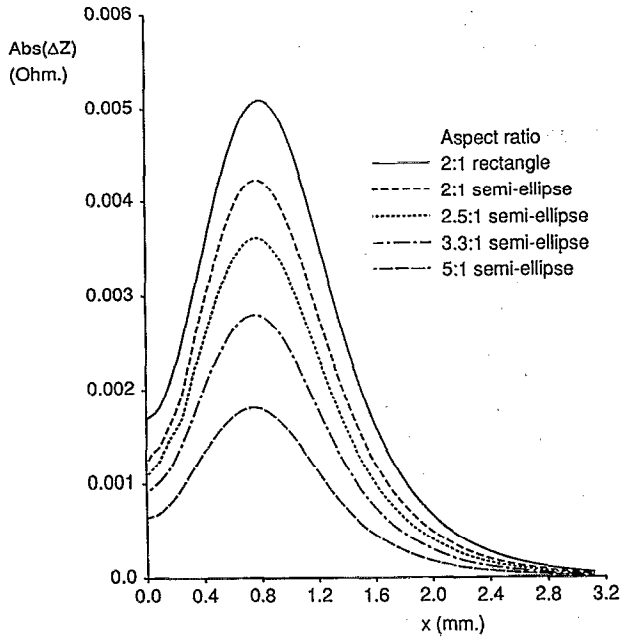

FIG. 4. Varation of probe impedance with position. Comparison of absolute impedance response for different flaws of the same length.

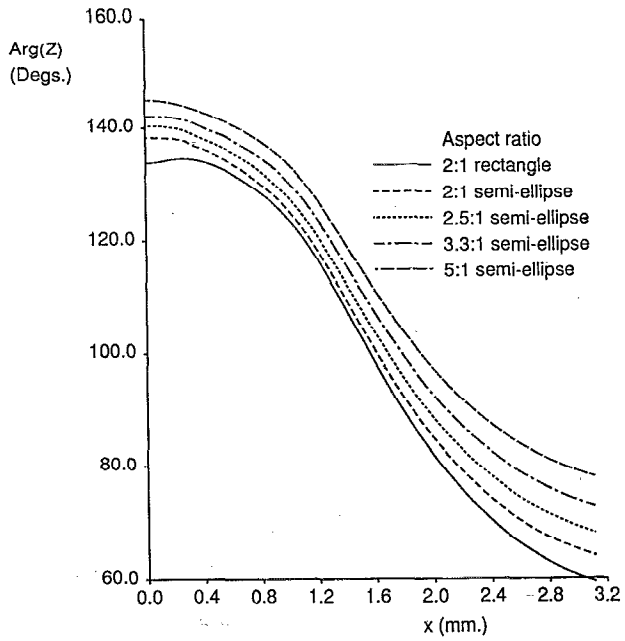

FIG. 5. Varation of probe impedance with position. Comparison of phase response for different flaws of the same length.

is displaced from the center by roughly one mean coil radius. The coil response is symmetrical about $x=0$, therefore a complete plot, including negative values of x, shows two peaks separated by a distance approximately equal to the mean coil diameter. Predictions are given for a number of volume element structures from a coarse array of $1\times7\times4$ cells, only 84 unknowns, to a $3\times15\times16$ grid with 2160 unknowns. Either 1 or 3 elements span the slot opening with improved accuracy found when 3 layers of volume elements are across the slot. The best predictions here are well within the estimated experiment error of 5%, therefore the small-phase discrepancy between experiment and the $3\times15\times16$ predictions, Fig. 3, is probably not significant.

The prediction of eddy-current probe signals from interaction with a prescribed flaw is referred to as a forward problem in contrast to inverse problems where the signal is given and the flaw parameters must be found. Inversion is the central task of NDE, but it is a task that is inextricably linked to forward models of one kind or another. As an elementary approach to inversion one can simply run the forward model repeatedly and try to match solutions to given data. At an advanced level, one might make a direct attack on an integral formulation of a full nonlinear inversion problem. The success of any approach, whatever the details, depends on whether or not the observations are sensitive to the flaw parameters sought. To illustrate the relationship between flaw geometry and the eddy-current probe response, a number of calculations have been made showing the signal variation due to a variety of flaws.

Figures 4 and 5 show the variation of impedance with probe position for various slots of the same length but having different aspect ratios. The parameters of the calculation are given in Table II where the flaw parameters are referred to as the First Series. The skin depth here is 0.558 mm and the aspect ratio defined as the ratio of flaw length to depth. Four of the slots are semielliptical and one is rectangular. The shape of the response for a rectangular slot does not differ by very much from the overall shape of the response for the semielliptical slots. There are, however, differences in absolute impedance and phase as the aspect ratio is varied. Figures 6 and 7 compare the predicted response for a number of semielliptical slots of the same depth but differing in length (Table II, Second Series). A dramatic variation in impedance is seen in this case depending on the relative size of the flaw and coil. If

TABLE II. Parameters for compararison of response due to various flaws.

Coil parameters	
Inner radius (ρ_1)	0.50 mm
Outer radius (ρ_2)	0.75 mm
Length ($z_b - z_a$)	3.0 mm
Number of turns	40
Liftoff (z_a)	0.1 mm
Frequency	1.0 MHz
Specimen parameter	
Conductivity (σ)	8.13×10^5 s/m
Flaw parameters	
First series	
Length ($2c$)	1.2 mm
Depth (h)	0.6, 0.48, 0.36, 0.24 mm
Width (w)	0.05 mm
Second series	
Length ($2c$)	0.8, 1.6, 2.4, 3.2 mm
Depth (h)	0.36 mm
Width (w)	0.05 mm

Downloaded 10 May 2004 to 129.186.200.45. Redistribution subject to AIP license or copyright, see http://jap.aip.org/jap/copyright.jsp

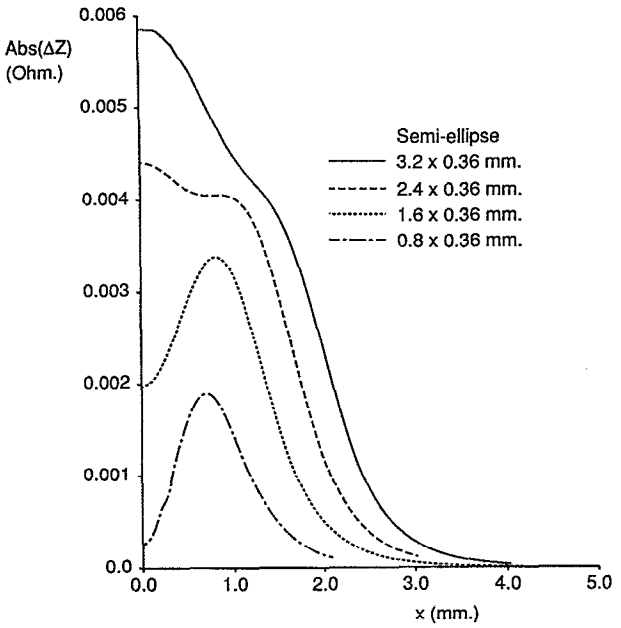

FIG. 6. Varation of probe impedance with position. Comparison of absolute impedance variation for semielliptical flaws of the same depth but with different lengths.

the flaw is small, the minimum in the absolute impedance at $x=0$ is very marked but the minimum becomes a maximum at $x=0$ if the flaw length is substantially greater than the coil diameter. Although the eddy-current distribution has not been calculated, one can speculate that the change from a minimum to a maximum at $x=0$ may be associated with the tendency of the induced current to pass below a long flaw rather than around a short one.

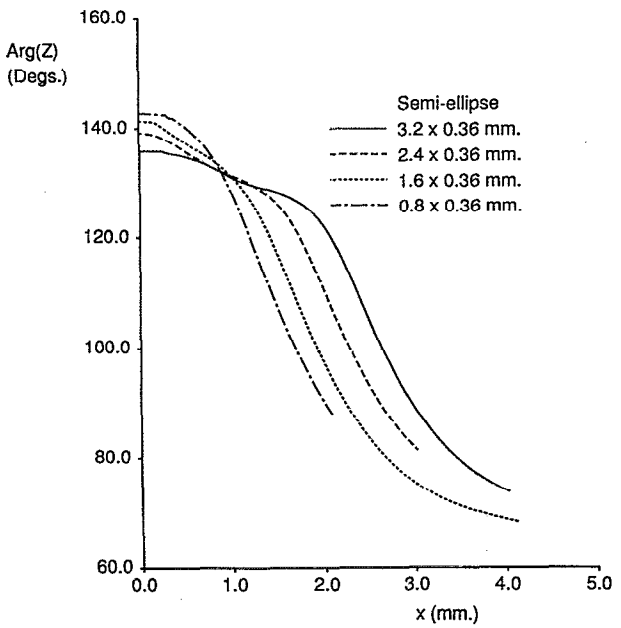

FIG. 7. Varation of probe impedance with position. Comparison of the phase variation for semielliptical flaws of the same depth but with different lengths.

VIII. CONCLUSION

A theory for predicting eddy-current coil impedance due to the presence of a three-dimensional flaw in a con'ductor has been developed. Numerical calculations based on the theory have been carried out using the moment method to derive a discrete system of linear equations and a conjugate gradient algorithm to get an approximate solution. Extensive use of fast Fourier transforms, in the iteration procedure, give efficient coding of probe-flaw interaction allowing problems to be solved that require a large number of unknowns. Predictions of probe response for a simulated defect show good agreement with experiment.

ACKNOWLEDGMENTS

The authors would like to thank Dr. S. K. Burke of Aeronautical Research Laboratories, Melbourne, Australia, for the use of data prior to publication. One of us (J. R. B.) is supported by the Procurement Executive, Ministry of Defense U.K. Another of us (S. A. J.) is supported by Nuclear Electric, plc. The international collaboration was facilitated by The Technical Cooperation Program, PTP-5.

[1] M. L. Burrows, Ph.D. dissertation, University of Michigan, University Microfilms, Ann Arbor, Michigan, 1964.
[2] J. R. Bowler, in *Review of Progress in Quantitative Nondestructive Evaluation,* edited by D. O. Thompson and D. E. Chimenti (Plenum, New York, 1987), p. 185.
[3] C.-T. Tai, *Dyadic Green's Functions in Electromagnetic Theory* (Intext, 1971).
[4] R. F. Harrington, *Field Computation by Moment Methods* (Macmillan, New York, 1968).
[5] D. McA. McKirdy, J. Nondestruct. Eval. **8**, 45 (1989).
[6] T. K. Sarkar, E. Arvas, and S. M. Rao, IEEE Trans. Antennas Propag.
[7] R. F. Harrington, *Time Harmonic Electromagnetic Fields* (McGraw-Hill, New York, 1961).
[8] J. R. Bowler, L. D. Sabbagh, and H. A. Sabbagh, IEEE Trans. Magn. **MAG-25**, No. 3, 2650 (1989).
[9] J. R. Bowler, J. Appl. Phys. **61**, 833 (1987).
[10] A. P. Raiche and J. H. Coggon, J. R. Astron. Soc. **36**, 363 (1974).
[11] A. Banos, Jr., *Dipole Radiation in the Presence of a Conducting Half Spaced* (Pergamon, Oxford, 1966), p. 135.
[12] I. S. Gradshteyn and I. M. Ryzhik, *Tables of Integrals Series and Products,* 4th. ed. (Academic, New York, 1965), see integral 6.637.
[13] M. Abramowitz and I. A. Stegun, *Handbook of Mathematical Fuctions with Formulas, Graphs, and Mathematical Tables* (Wiley, New York, 1970), 10th printing, pp. 379–385.
[14] W. H. Press, B. P. Flannery, S. A. Teukolsky, and W. T. Vetterling, *Numerical Recipes, The Art of Scientific Computing* (Cambridge University, Cambridge, 1988).
[15] S. Lee, J. B. Boersma, C. Law, and G. A. Deschamps, IEEE Trans. Antennas Propag. **AP-28**, 311 (1986).
[16] S. A. Jenkins and J. R. Bowler (unpublished).
[17] I. S. Gradshteyn and I. M. Ryzhik, *Tables of Integrals Series and Products,* 4th ed. (Academic, New York, 1965); see integral 6.561.
[18] M. Hestenes, *Conjugate Direction Methods in Optimization* (Springer, New York, 1980).
[19] J. Stoer and Bulirsch, *Introduction to Numerical Analysis* (Springer, New York, 1980).
[20] S. K. Burke, J. Nondestruct. Eval. **7**, 35 (1988).

Downloaded 10 May 2004 to 129.186.200.45. Redistribution subject to AIP license or copyright, see http://jap.aip.org/jap/copyright.jsp